International Journal of General Medicine

Dovepress
Taylor & Francis Group

Open Access Full Text Article

ORIGINAL RESEARCH

Identification and Validation of Key Genes Involved in the Coupling of Mitochondria-Associated Endoplasmic Reticulum Membrane in Hemorrhoidal Disease

Lihua Mao*, Zhiying Rao*, Yanru Wang, Jun Yang, Junmei He, Zhi Zheng, Lanyu Chen

Department of Anorectal Surgery, Jiangxi Provincial People's Hospital, The First Affiliated Hospital of Nanchang Medical College, Nanchang, Jiangxi, 330006, People's Republic of China

*These authors contributed equally to this work

Correspondence: Zhiying Rao, Department of Anorectal Surgery, Jiangxi Provincial People's Hospital, The First Affiliated Hospital of Nanchang Medical College, Nanchang, Jiangxi, 330006, People's Republic of China, Tel +86 15505998855, Email 1522896861@qq.com

Background: Hemorrhoidal disease (HD) is the most prevalent rectal disorder, with various cellular processes influenced by the mitochondria-associated endoplasmic reticulum membrane (MAM). Potential therapeutic mechanisms for HD may be associated with MAM. This study aims to identify key genes linked to MAM in HD and to provide novel therapeutic targets.

Methods: Transcriptome data and MAM-related genes (MAM-RGs) were obtained from the Gene Expression Omnibus (GEO) database and relevant literature. Differential expression analysis and single-sample Gene Set Enrichment Analysis (ssGSEA) scores were initially employed to identify candidate genes. Key genes were further refined using Least Absolute Shrinkage and Selection Operator (LASSO) and Protein-Protein Interaction (PPI) networks. A nomogram based on these key genes was developed and assessed. Additionally, CIBERSORT algorithms were utilized to evaluate immune cell infiltration abundance, differences, and correlations in the samples. Finally, the expression of key genes was validated via reverse transcription-quantitative PCR (RT-qPCR).

Results: Differential expression analysis identified 956 differentially expressed genes (DEGs), and ssGSEA identified 143 differentially expressed MAM-RGs. A total of 50 candidate genes were selected through their intersection. Machine learning identified two key genes, *MUC16* and *DEFA5*. A nomogram with strong predictive capability was constructed. Immune cell analysis revealed two types of differential immune cells—activated dendritic cells and plasma cells—where activated dendritic cells were more highly expressed in the case group, and plasma cells showed a strong positive correlation with *DEFA5*. Additionally, *MUC16* was significantly overexpressed in patients with HD, while *DEFA5* exhibited down-regulation compared to controls.

Conclusion: This study identifies *MUC16* and *DEFA5* as key genes associated with HD and MAM and presents a predictive nomogram with high accuracy. These findings provide novel insights into the mechanisms and potential treatment targets for HD.

Keywords: hemorrhoidal disease, mitochondria-associated endoplasmic reticulum membrane, nomogram, immune infiltration

Introduction

Hemorrhoidal disease (HD) represents the most prevalent rectal condition, affecting up to 39% of the population,[1] with a peak incidence in individuals aged 45–65 years.[2] HD is characterized by the inflammation and prolapse of vascular tissues within the anal canal, often leading to high recurrence rates following treatment.[3] Common symptoms include anal itching, pain, and the development of lumps at the anal margin due to thrombosis or strangulation.[4] It is estimated that 75% of the global population will experience HD at some point, with severe cases necessitating interventions such as medication, surgery, or other treatments.[5] Risk factors for HD include a low-fiber diet, inadequate water intake, pregnancy, constipation, prolonged straining, increased intra-abdominal pressure, and weakened muscle support.[2,6]

Received: 24 December 2024
Accepted: 24 May 2025
Published: 31 May 2025

Graphical Abstract

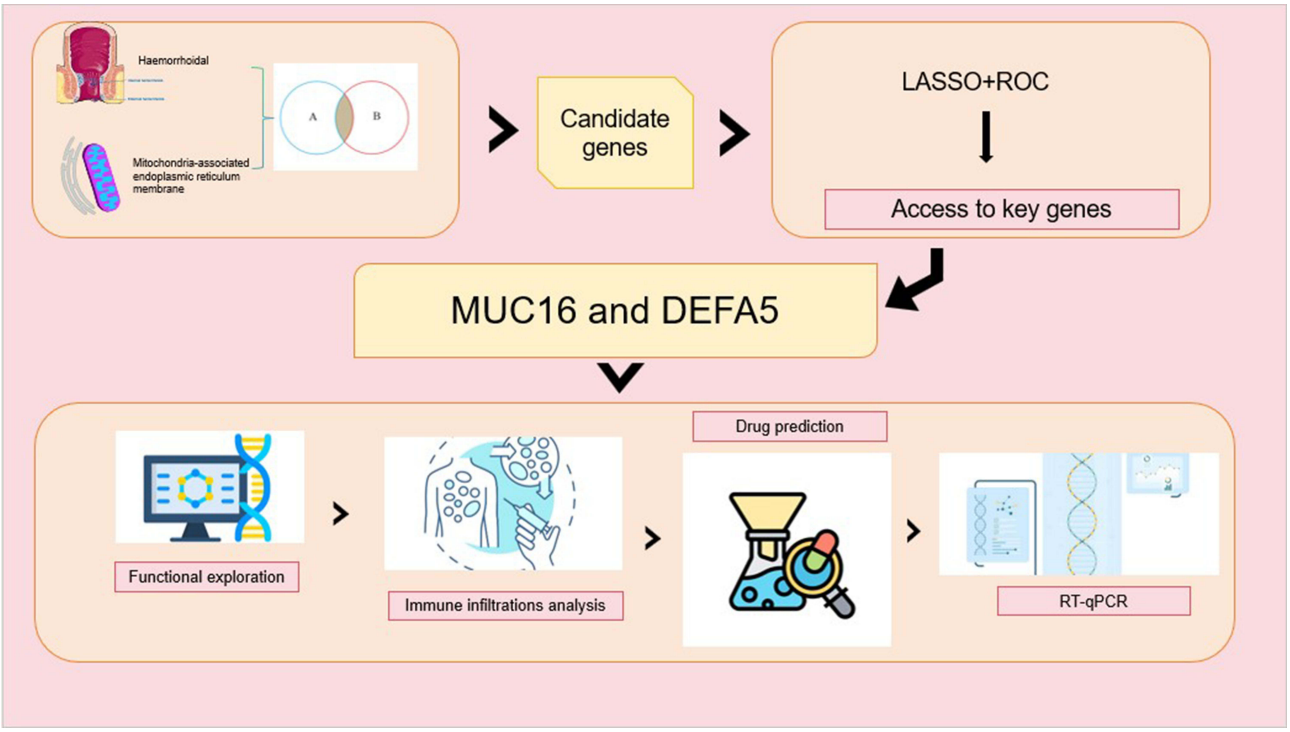

Despite these known associations, the molecular mechanisms underlying HD remain poorly understood, underscoring the need for further research to elucidate its pathogenesis and potential links to other diseases.

Mitochondria interact with cellular structures such as the Golgi apparatus, endoplasmic reticulum (ER), lipid droplets, and peroxisomes. The mitochondrial-endoplasmic reticulum contact sites, or mitochondria-associated ER membranes (MAMs), are critical for regulating lipid synthesis and transport, Ca^{2+} transfer and signaling, mitochondrial dynamics, mitosis, apoptosis, the ER stress response, and inflammation.[7] MAMs play a vital role in maintaining normal cellular function. Additionally, MAMs, through miRNA regulation, can influence inflammatory diseases and contribute to cellular stress, which may lead to conditions like diabetes, inflammation, neurodegeneration, and autoimmune disorders.[8,9] MAMs also present a promising target for cardiovascular disease treatment and are involved in regulating metabolic disorders, including those associated with HD.[10,11] The underlying mechanisms of HD treatment are linked to processes such as cell migration, proliferation, motility, and apoptosis.[12] Therefore, we hypothesize that MAM-related genes may influence neurodegeneration by regulating mitochondrial function, and are expected to identify novel therapeutic targets for HD, providing innovative strategies for its treatment.

This study leveraged transcriptomic data and MAM-related genes (MAM-RGs) to identify differentially expressed candidate genes. Through the construction of a protein interaction network and integration with machine learning, two key genes were pinpointed. A nomogram based on these genes demonstrated robust predictive power. Furthermore, bioinformatics analyses were employed to examine the biological pathways associated with these key genes, their molecular regulatory networks, and potential targeted drugs. This research provides a comprehensive foundation for understanding the mechanisms of HD and identifies new therapeutic targets for its management.

Materials and Methods

Data Sources

The training set (GSE154650, platform: GPL20301) was sourced from the Gene Expression Omnibus database (GEO, https://www.ncbi.nlm.nih.gov/geo/). The disease group (case group) comprised 20 hemorrhoidal anal canal tissue samples, while the control group consisted of 18 healthy anal canal tissue samples from individuals who had undergone anal fissure surgery. A total of 28 MAM-related genes (MAM-RGs) were identified from the literature,[13] including *ACAT1, ACSL4, ATAD3A, ATP2A2, BCAP3A, CANX, CAV1, DGAT2, DNMIL, FIS1, FUNDC1, HSPA9, ITPR2, ITPR3, MFN1, MFN2, NDUFS4, PACS2, PARK2, PDK4, PEMT, PINK1, PSEN2, RMDN3, SEPN1, SERAC1, VAPB*, and *VDAC1*.

Identification of Differential Expression Genes (DEGs)

To identify DEGs in the case and control groups within the GSE154650 dataset, differential analysis was performed using the R package "DESeq2" (v 1.42.0).[14] A fold change (FC) and P value threshold were applied to filter the DEGs ($|\log_2 FC| > 1.5$, $P < 0.05$), which were labeled as DEGs1 for subsequent analysis. The "ggplot2" package (v 3.5.1)[15] was used to generate volcano and heatmaps of DEGs1, sorted by $\log_2 FC$ value from highest to lowest, with the top 10 upregulated and downregulated DEGs labeled in the volcano plots. Next, the expression differences of MAM-RGs between the case and control groups were compared. The R package "GSVA" (v 1.50.0)[16] was used to compute the single-sample Gene Set Enrichment Analysis (ssGSEA) scores for the differentially expressed MAM-RGs. Based on the median ssGSEA scores, the dataset was divided into high- and low-score groups. Differential gene expression analysis was then conducted using "DESeq2" (v 1.42.0), with thresholds of $|\log_2 FC| > 1.5$ and $P < 0.05$ to identify DEGs2 for further analysis. The "ggplot2" package (v 3.5.1) was again used to visualize DEGs1 and DEGs2 through separate volcano plots.

Identification and Functional Enrichment of Candidate Genes

To identify the genes common to DEGs1 and DEGs2, the intersection of these two sets was determined using the "VennDiagram" package (v 1.7.3),[17] and these genes were labeled as candidate genes for further analysis, as shown in the Venn diagram. Additionally, to gain insights into the potential biological functions of the candidate genes, the "clusterProfiler" package (v 4.7.1.003)[18] was used for Gene Ontology (GO) ($P < 0.05$) and Kyoto Encyclopedia of Genes and Genomes (KEGG) pathway enrichment analysis ($P < 0.05$). The results were ranked by P values from largest to smallest to identify the pathways and potential functions associated with the candidate genes.

Using Protein-Protein Interaction (PPI) and Machine Learning to Distinguish Key Genes

To explore the protein-level interactions of candidate genes, a PPI network was constructed using the Search Tool for the Retrieval of Interacting Genes (STRING, http://string-db.org) with an interaction score threshold of > 0.4. After removing isolated nodes, the PPI network was visualized using Cytoscape (v 3.9.1).[19] To identify key genes with significant roles among the candidate genes, three algorithms—BottleNeck, Closeness, and Stress—within the CytoHubba plugin were used to evaluate the importance of each gene. The top 15 genes identified by these algorithms were selected for further analysis. The R package "VennDiagram" (v 1.7.3) was used to take the intersection of the top 15 genes from the BottleNeck, Closeness, and Stress algorithms. These intersected genes were labeled as feature genes-PPI for subsequent analysis and visualization. Additionally, Least Absolute Shrinkage and Selection Operator (LASSO) regression analysis was performed using the expression data of candidate genes through the R package "glmnet" (v 4.1.1)[20] to select feature genes-LASSO. The intersection of feature genes-PPI and feature genes-LASSO was then identified using the "VennDiagram" package (v 1.7.3). Receiver Operating Characteristic (ROC) curves for the intersected genes were plotted using the R package "pROC" (v 1.18.0),[21] and the Area Under the Curve (AUC) was calculated. Genes with AUC > 0.7 were considered key genes.

Gene Set Enrichment Analysis (GSEA)

To further explore the biological functions and pathways of the key genes, Spearman correlation analysis was first conducted between all genes and the key genes using the R package "corrplot" (v 0.92).[22] Next, "mh.all.v2023.2.mm.

symbols.gmt" from the Molecular Signature Database (MsigDB, https://www.gsea-msigdb.org/gsea/msigdb) was used as the background gene set. GSEA was performed using the R package "clusterProfiler" (v 4.7.1.003),[18] with the enrichment results sorted by P value from smallest to largest. The top 5 enriched pathways were visualized using the R package "ggplot2" (v 3.4.4).

Constructing Nomogram for Key Genes

To evaluate the clinical diagnostic performance of key genes, the R package "rms" (v 6.5.0)[23] was utilized to construct a nomogram based on key genes from the GSE154650 dataset. Each key gene was assigned a score (Point), and the overall incidence of the disease was inferred from the Total Point. The accuracy and validity of the nomogram model in predicting disease occurrence were then assessed. The calibration curve was plotted using the calibrate function in the "rms" package (v 6.5.0) to compare the predicted values with the true values. The R package "pROC" (v 1.18.0)[21] was employed to generate the ROC curve, with an AUC closer to 1 indicating a more accurate diagnostic performance. Finally, Decision Curve Analysis (DCA) was conducted to assess the net benefit of the constructed nomogram.

Immunoinfiltration Analysis

Immune cell infiltration analysis can offer insights into personalized hemorrhoid treatment. The abundance of 22 immune cell types[24] in the case and control groups was assessed using the CIBERSORT algorithm[25] on all samples from the GSE154650 dataset. Samples with $P > 0.05$ were excluded from visualization, and differences in immune cell infiltration between the case and control groups were considered significant at $P < 0.05$. Additionally, the R package "Mental" (v2.2.5)[26] was used to evaluate the correlation between key genes and differential immune cells, with |correlation (cor)| > 0.3 and $P < 0.05$ used as thresholds for significance.

Building Regulatory Networks for Key Genes

To investigate the molecular regulatory mechanisms of key genes, the Human Transcription Factors and Their Targets database (hTFtarget, http://bioinfo.life.hust.edu.cn/hTFtarget) was employed to predict transcription factors (TFs) associated with key genes. The experimentally validated microRNA-target interactions database (miRTarBase, http://mirtarbase.mbc.nctu.edu.tw/index.html) was used to identify microRNAs (miRNAs) linked to key genes. Moreover, the Encyclopedia of RNA Interactome database (ENCORI, https://starbase.sysu.edu.cn/) was utilized to predict the interactions between RNA-binding proteins (RBPs) and key genes, using the criteria of clusterNum≧2 and clipExpNum≧2. These results were visualized using Cytoscape (v 3.9.1).[19]

Drug Forecasting

To explore potential drug targets for key genes, drugs were predicted using the Drug-Gene Interaction Database (DGIdb, https://www.dgidb.org/). A network incorporating drugs, key genes, and differential immune cells was constructed based on these predictions, and the network was visualized using the R package "plotly" (v 5.23.0).[27]

Reverse Transcription-Quantitative PCR (RT-qPCR)

To verify the consistency of key gene expression with bioinformatics results, RT-qPCR was performed. Anal canal tissue samples were collected from five clinical patients who underwent hemorrhoidal surgery and five who underwent anal fissure surgery. Total RNA was extracted using the Trizol method[28] and reverse-transcribed to cDNA. The expression levels of key genes were quantified using the $2^{-\Delta\Delta Ct}$ method[29] with GAPDH as the control, and statistical significance was determined at $P < 0.05$. Primer sequences are listed in Supplementary Table 1.

Statistical Analysis

Bioinformatics analysis was conducted using R language (v 4.2.2). The Wilcoxon test was used to compare differences between the two groups, with $P < 0.05$ indicating statistical significance.

Results

Fifty Candidate Genes Identified

After applying threshold screening, a total of 956 DEGs1 were identified in the GSE154650 dataset, comprising 387 up-regulated genes and 569 down-regulated genes (Figure 1A and B). Subsequently, 26 MAM-RGs were identified, with

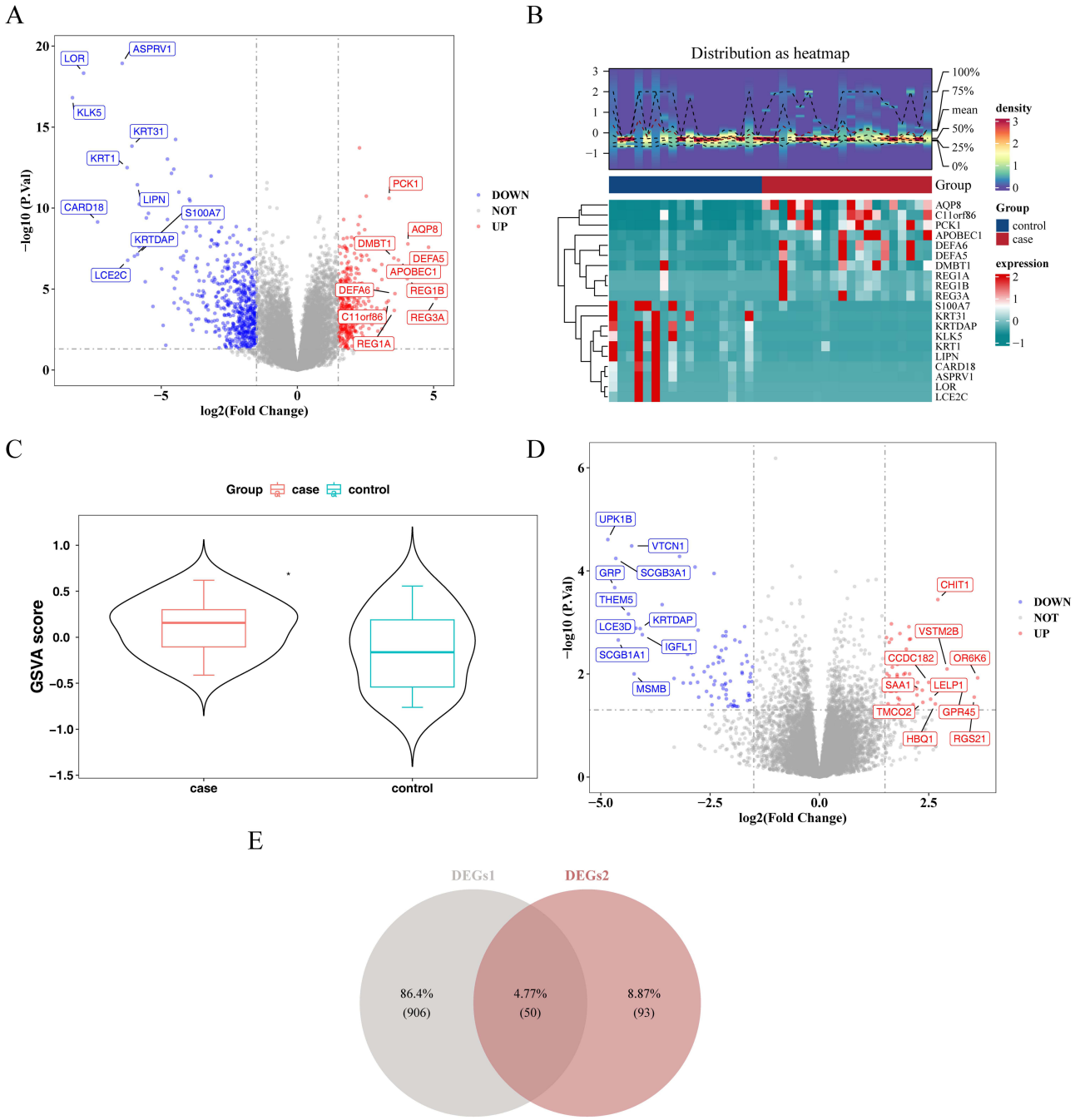

Figure 1 Screening and identification of candidate genes. (**A**) Volcano Plot of Differentially Expressed Genes: Red dots represent significantly upregulated genes, blue dots represent significantly downregulated genes, and gray dots represent genes without significant differential expression. The names of the top 10 most significantly upregulated and downregulated genes are displayed. (**B**) Heatmap of Differentially Expressed Genes: The upper section features a density heatmap showing the expression levels of differentially expressed genes across samples, with lines representing five quantiles and the mean. The lower section displays a heatmap illustrating the expression of differentially expressed genes across the samples. (**C**) Differences in MER Scores Between the Case Group and Control Group: Blue color indicates the normal group, while red color indicates the disease group. (**D**) Volcano Plot of Differentially Expressed Genes: A second volcano plot showing the distribution and significance of differential gene expression. (**E**) Venn Diagram of Candidate Gene Identification: A Venn diagram illustrating the overlap and identification of candidate genes. An asterisk (*) was usually used to indicate that $P < 0.05$.

https://doi.org/10.2147/IJGM.S511281

ACAT1, DGAT2, and *PINK1* showing significant expression differences between the case and control groups (Supplementary Table 2). The ssGSEA scores for these three genes were significantly higher in the case group compared to the control group ($P < 0.05$) (Figure 1C). The disease samples were then divided into high- and low-scoring groups, with 10 samples in each group (median score = 0.007540664). Analysis of variance revealed 143 DEGs2 between the two groups, with 62 up-regulated genes and 81 down-regulated genes in the scoring group (Figure 1D). Finally, based on the intersections of DEGs1 and DEGs2, 50 candidate genes were obtained (Figure 1E).

Functional Enrichment of Candidate Genes and PPI Network Building

The 50 candidate genes were enriched in 215 GO terms. Among these, 187 biological process (BP) terms were enriched, including response to lipopolysaccharide, response to bacterial molecules, and cellular response to lipopolysaccharide. Four terms were enriched in cellular component (CC), with significant associations to the Golgi lumen, ciliary rootlet, and lamellar body. Additionally, 24 molecular function (MF) terms were enriched, including cytokine activity, cytokine receptor binding, and G protein-coupled receptor binding (Figure 2A and Supplementary Table 3). In KEGG, five related pathways were identified, with candidate genes being significantly associated with immune system, bacterial infectious diseases, digestive system, signaling molecules and interactions, and the endocrine system pathways (Figure 2B). Furthermore, the PPI network of the 50 candidate genes revealed 22 interactions with a total of 26 edges (Figure 2C). Notably, MUC5AC and LCE3D interacted with five other proteins, while MUC16 and S100A7A each interacted with four other proteins.

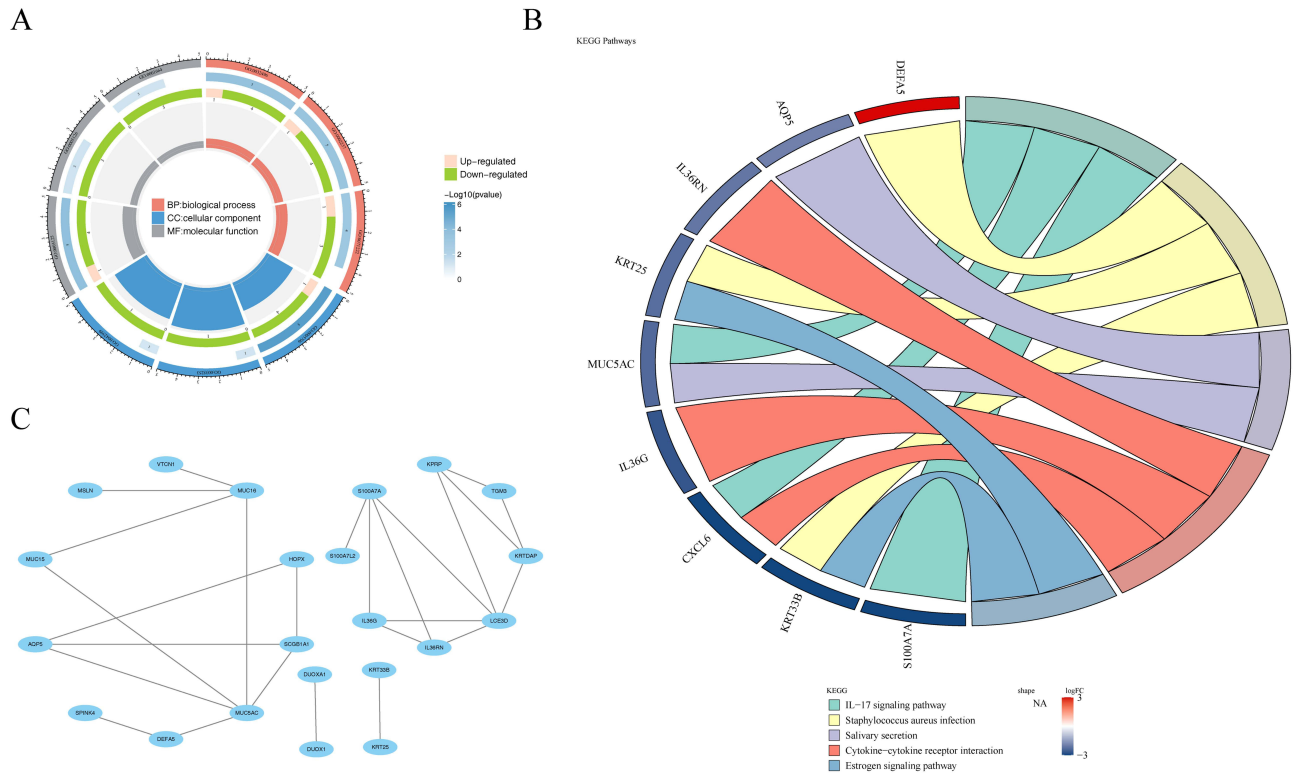

Figure 2 GO and KEGG enrichment analyses of candidate genes and construction of the PPI network. (**A**) GO Enrichment Analysis of Candidate Genes: The outermost layer represents the GO annotation ID, with red indicating biological processes, blue representing cellular components, and yellow indicating molecular functions. The second layer shows the significance level, with color intensity representing the p-value, and the length and width of the segments, along with the numbers, indicate the number of genes enriched in each function. The third layer displays the number of upregulated and downregulated genes enriched in each function, with colors distinguishing between up- and downregulation. (**B**) KEGG Enrichment Analysis of Candidate Genes: The left side displays the names of enriched genes, with color intensity representing the fold change (logFC), where darker colors indicate larger fold changes. The right side shows the enriched pathways, with different colors corresponding to different pathways. Pathway names are listed below the diagram under "Terms". The size of the color blocks varies according to the number of genes enriched in each pathway; larger blocks represent pathways with more enriched genes. (**C**) PPI Network Diagram: The nodes represent genes, and the edges represent interactions between the genes.

The Key Genes MUC16 and DEFA5 Were Identified and Obtained

The top 15 genes identified through three algorithms (BottleNeck, Closeness, and Stress) were intersected (Figure 3A–C), resulting in 11 feature genes-PPI: *MUC5AC, LCE3D, MUC16, S100A7A, DEFA5, SCGB1A1, KRTDAP, MUC15, IL36G, VTCN1*, and *HOPX* (Figure 3D). Meanwhile, LASSO regression analysis of the 50 candidate genes indicated that the model's error rate was minimized when lambda.min was 0.02883683 (Figure 3E), leading to the identification of 10 feature genes-LASSO: *DEFA5, CXCL6, SPINK4, FIGF, AQP5, HMP19, MUC16, TGM3, TCL1A*, and *SPACA1* (Figure 3F). The intersection of feature genes-PPI and feature genes-LASSO revealed two common genes: *MUC16* and *DEFA5* (Figure 3G). ROC curves were plotted for these intersecting genes, with *MUC16* achieving an AUC of 0.756 and *DEFA5* achieving an AUC of 0.856 (Figure 3H), indicating that these key genes effectively distinguish case samples from control samples. Consequently, *MUC16* and *DEFA5* were determined as the final key genes.

Functional Exploration of MUC16 and DEFA5

In the GSE154650 dataset, GSEA revealed that *MUC16* was significantly associated with pathways including drug metabolism by other enzymes, oxidative phosphorylation, Parkinson's disease, pentose and glucuronate interconversions, and starch and sucrose metabolism (Figure 4A). *DEFA5* was found to be significantly correlated with pathways such as ascorbate and aldarate metabolism, drug metabolism by enzymes, maturity-onset diabetes of the young, N-glycan biosynthesis, and pentose and glucuronate interconversions (Figure 4B). Additionally, both *MUC16* and *DEFA5* were significantly associated with the pathways related to drug metabolism by other enzymes and pentose and glucuronate interconversions.

Construction and Evaluation of Nomogram with MUC16 and DEFA5

In the nomogram plot for predicted HD prevalence based on key genes, the points for *MUC16* and *DEFA5* were marked with red-dotted lines (Figure 5A). The calibration curve showed no significant difference between the anticipated and true values (Figure 5B), and the nomogram's AUC was 0.88 (Figure 5C), indicating that the model built with key genes had high prediction accuracy and disease prediction capability. Furthermore, the DCA curve demonstrated that the net benefit of the nomogram was consistently greater than zero and higher than the net benefit of the individual key genes (Figure 5D). Overall, the nomogram model displayed favorable predictive performance.

Analysis of 22 Immune Cell Infiltrations

Infiltration analysis of 22 immune cell types in the case and control groups is shown in Figure 6A. The highest level of infiltration in both groups was observed in resting memory CD4 T cells. Activated dendritic cells and plasma cells exhibited significant differences between the groups, with their infiltrated scores being down-regulated in the case group and up-regulated in the control group (Figure 6B). Additionally, a strong positive correlation was observed between plasma cells and *DEFA5* (cor = 0.5321, $P < 0.01$) (Figure 6C).

Construction of an mRNA-TF-miRNA Network for DEFA5 and MUC16

The regulatory network analysis visualized the transcriptional regulatory relationships of the two key genes, *DEFA5* and MUC16. *DEFA5* was predicted to be regulated by 58 TFs, while *MUC16* was predicted to be regulated by 18 TFs. After merging and removing duplicates, 26 unique TFs were identified. Furthermore, 39 miRNAs were predicted for *DEFA5* and 55 miRNAs for *MUC16*. Notably, *DEFA5* and *MUC16* together were regulated by three common TFs: LMNB1, DDX5, and SPI1, and 92 unique miRNAs were identified after filtering duplicates. The mRNA-TF-miRNA network is shown in Figure 7A. Additionally, *DEFA5* did not predict any RBPs, while 59 RBPs were predicted to interact with *MUC16*. After threshold filtering, 32 RBPs were retained, and the key gene-RBP interaction network was constructed and visualized (Figure 7B). The RBPs HNRNPK, CENPC, and RNPS1 exhibited the strongest interactions with *MUC16*.

A Total of 15 Targeted Drugs Were Predicted for DEFA5 and MUC16

Through the DGIdb, *DEFA5* and *MUC16* were predicted to target a total of 16 drugs. *DEFA5* was predicted to target 1 drug (sodium chloride), while *MUC16* was associated with 14 drugs. A network integrating differential immune cells

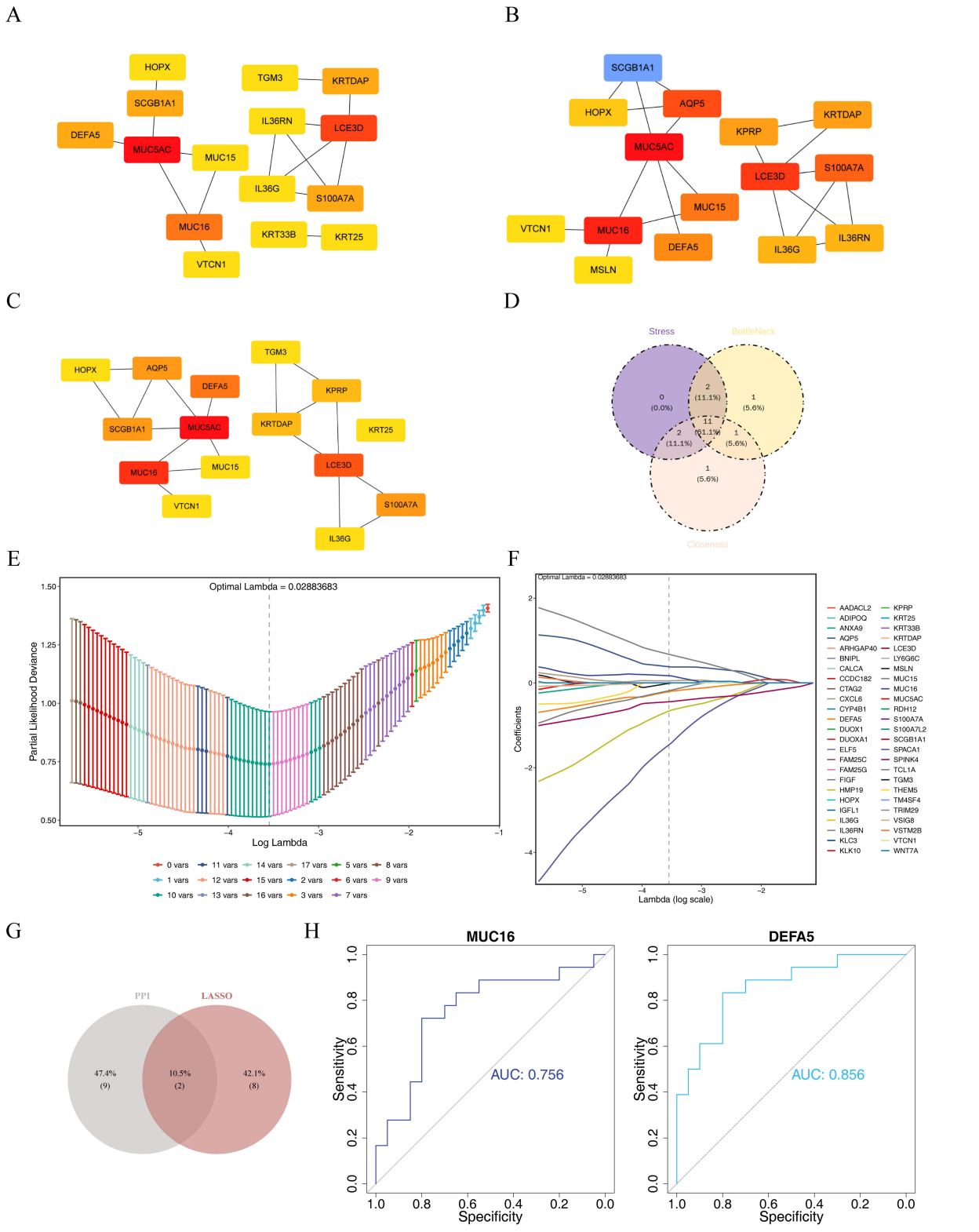

Figure 3 Screening and identification of key genes. (**A**–**C**) Top 15 results from the BottleNeck, Closeness, and Stress analyses of candidate genes. In the diagrams, gene nodes are represented by circles, and interactions between genes are depicted by lines. The color gradient of the gene nodes transitions from blue to red, signifying an increasing level of gene importance. (**D**) Venn diagram illustrating the feature gene 1 identified by all three algorithms. (**E**) Partial likelihood deviation plot from the LASSO analysis. The horizontal axis represents the logarithm of lambdas, while the vertical axis shows the partial likelihood deviation. (**F**) Coefficient plot from the LASSO analysis. The horizontal axis represents the logarithm of lambdas, and the vertical axis shows the variable coefficients. As lambdas increase, the coefficients approach zero, and variables with coefficients of zero are excluded when the optimal lambda is reached. (**G**) Venn diagram illustrating the identification of candidate key genes. (**H**) ROC analysis of candidate key genes in the training set GSE154650. The horizontal axis represents specificity, which measures the model's ability to correctly identify negative samples, while the vertical axis represents sensitivity (true positive rate), with values ranging from 0 to 1, indicating sensitivity from poor to optimal performance.

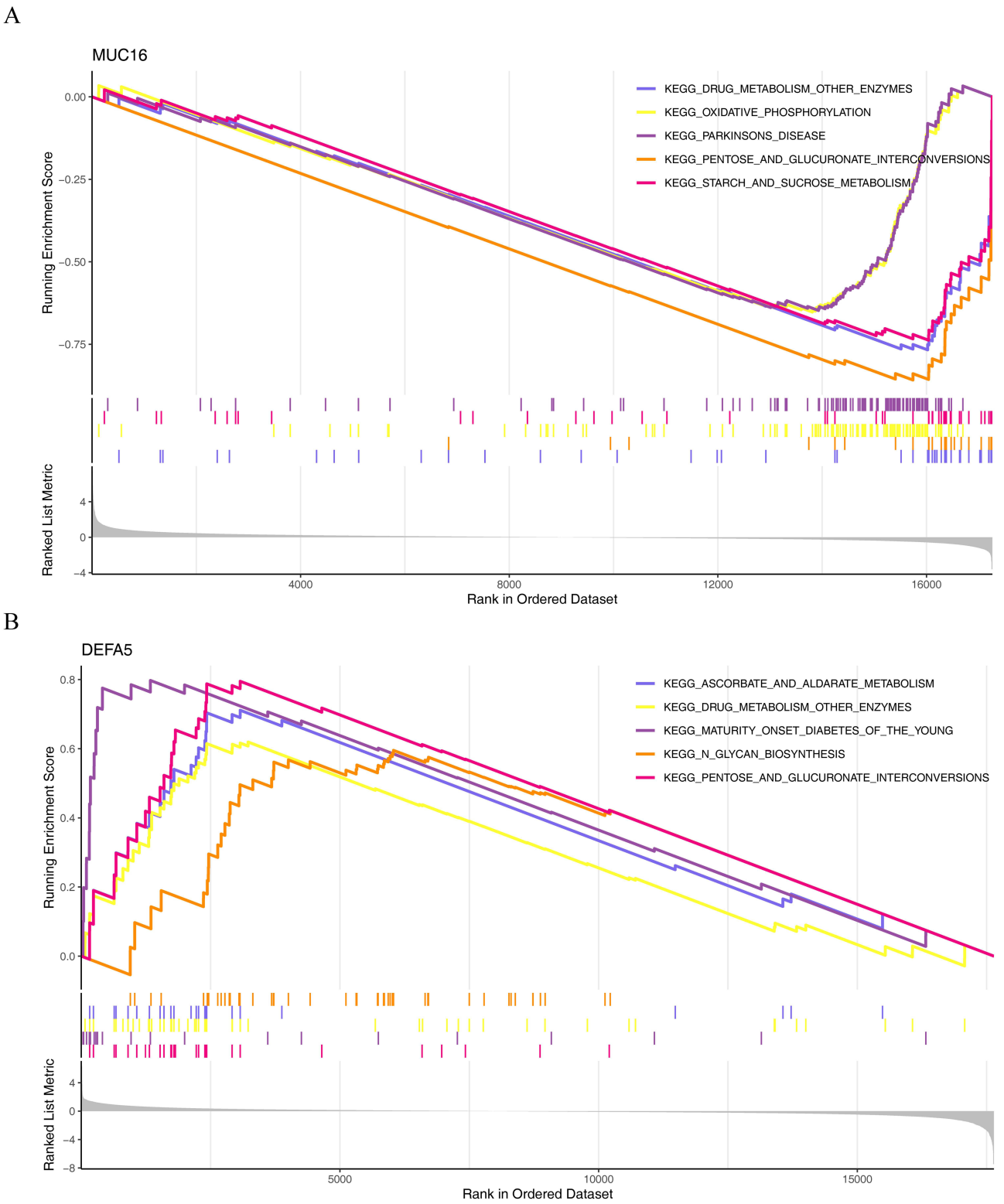

Figure 4 Functional enrichment analysis of key genes. (**A**) KEGG enrichment pathways for MUC16. (**B**) KEGG enrichment pathways for DEFA5. The upper section of each plot presents a line graph showing the enrichment scores for each gene. The horizontal axis represents the genes within the gene set, while the vertical axis represents the corresponding enrichment scores.

https://doi.org/10.2147/IJGM.S511281

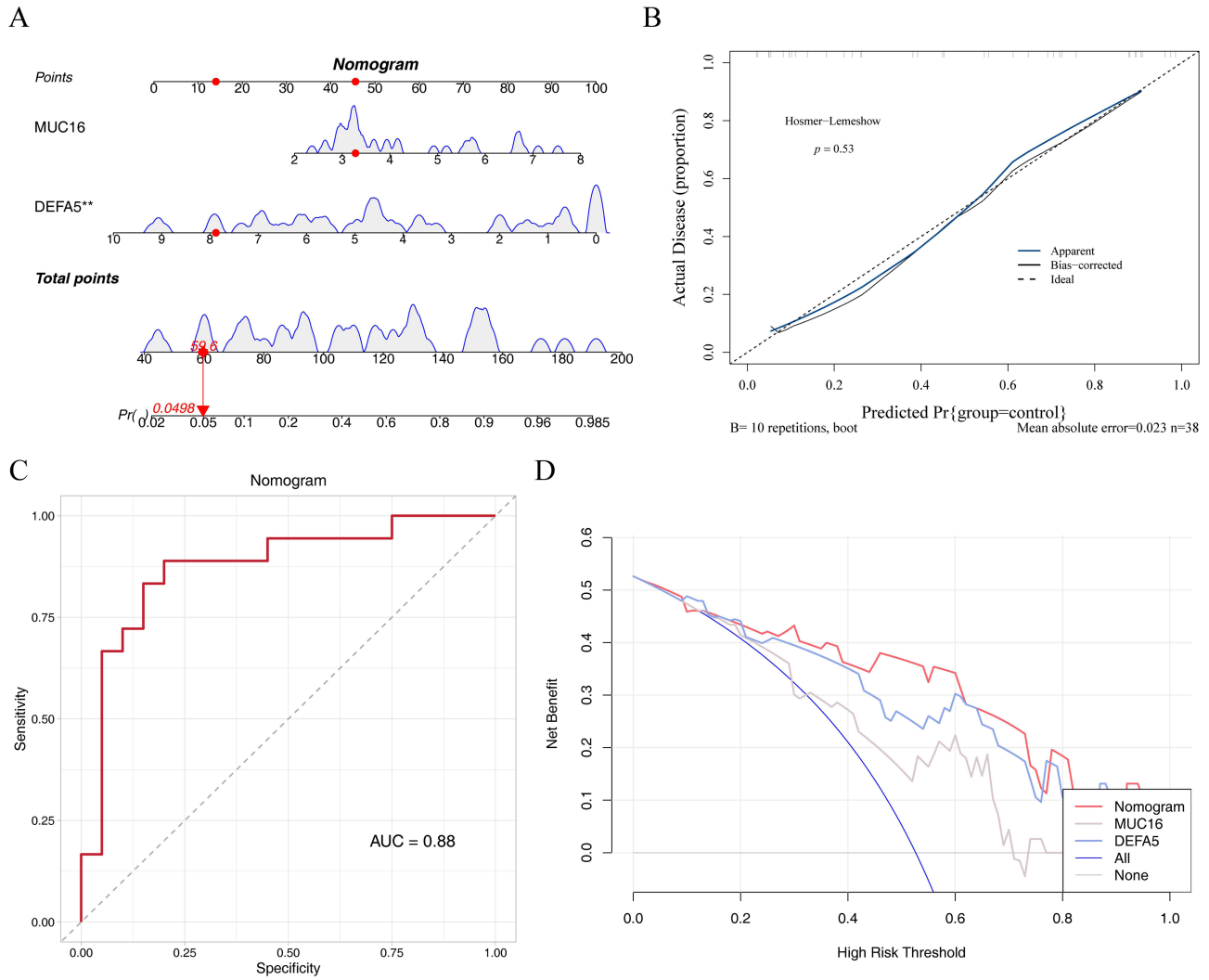

Figure 5 Construction and validation of nomogram. (**A**) Construction of nomograms. Each variable is represented by a line segment, with scales indicating the variable range. The length of the line reflects the contribution of the factor to the outcome event. The "Points" indicate the individual score corresponding to the value of each variable, while the "Total Points" represent the sum of all individual scores, calculated by adding the points for each variable. (**B**) Calibration curve for disease prediction using the nomogram. The horizontal axis represents the predicted probability of disease based on the nomogram, while the vertical axis represents the actual disease probability. The black dashed line represents perfect prediction. The blue solid line represents the entire cohort, and the black solid line, corrected for bias using bootstrapping (1000 repetitions), reflects the observed performance of the nomogram. (**C**) ROC curve for the nomogram. The horizontal axis represents specificity, and the vertical axis represents the true positive rate (sensitivity). AUC indicates the area under the ROC curve. (**D**) Decision curve for the nomogram. The horizontal axis represents risk, and the vertical axis represents net benefit. The different colored curves depict the net benefit of using various methods to predict disease.

(plasma cells and activated dendritic cells), drugs, and key genes was constructed, and the resulting drug-key gene-immune cell network is shown in Figure 7C.

RT-qPCR of MUC16 and DEFA5

RT-qPCR validation demonstrated that *MUC16* was significantly overexpressed in patients with HD (Figure 8A). In contrast, *DEFA5* showed down-regulation in patients with HD compared to controls, but the difference was not statistically significant (Figure 8B). These RT-qPCR results validate the bioinformatics findings and further elucidate the role of key genes in HD pathogenesis.

Discussion

HD is the most common rectal condition, characterized by inflammation of the anal canal and prolapse of bleeding vascular tissues. With a prevalence rate reaching up to 39% in the general population and a high recurrence rate after

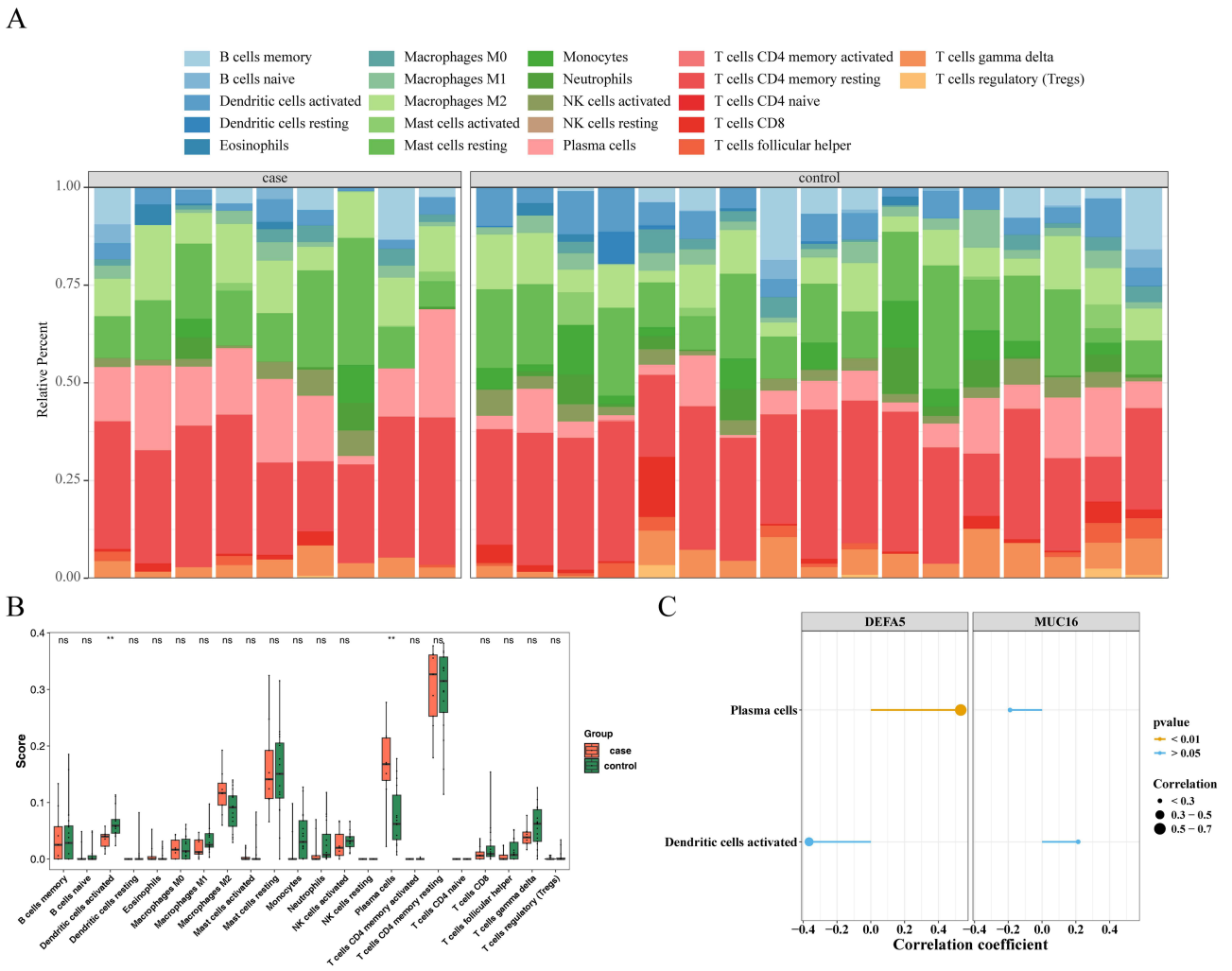

Figure 6 Immune infiltration analysis. (**A**) Proportional immune cell infiltration in the case and control groups. Different colors correspond to distinct immune cell types. The ordinate was represented the proportion of immune cells in different samples. "Case" and "control" were represented the HD group and the control group, respectively. (**B**) Infiltration status of 22 immune cell types in the case and control groups. The control group is represented by green, and the disease group is represented by blue., two asterisks (**) represented P < 0.01,. The "ns" was used to represent no significant difference. (**C**) Lollipop plot depicting the correlation between key genes and differential immune cells. Yellow indicates p < 0.01, and blue indicates p > 0.05. Larger circles represent stronger correlation values. The abscissa was marked with the correlation values, and the ordinate was represented the names of the diseases.

treatment,[1,3] HD poses a significant clinical challenge. Various cellular processes mediated by MAM, which result from the coupling of mitochondria and the endoplasmic reticulum, may play a role in the potential mechanisms underlying HD treatment. This study identified two key genes, DEFA5 and MUC16, providing theoretical support for understanding the pathogenesis of HD and highlighting new therapeutic targets for its management.

Studies suggest that DEFA5 is involved in protein folding, and members of the defensin family can interact with certain proteins to modulate their folding states.[30] Specifically, DEFA5 may bind to mHTT (mutant huntingtin), disrupting its normal folding and promoting misfolding/aggregation into neurotoxic inclusions. This process contributes to neuronal death and the onset of Huntington's disease (HD) symptoms.[31] Under physiological conditions, DEFA5 likely exerts neuroprotective effects by regulating intracellular signaling pathways.[32] For instance, it may modulate pathways associated with cell survival, proliferation, and differentiation, such as the MAPK cascade.[33] However, in HD patients, genetic mutations or other factors may impair DEFA5's normal function, preventing activation of these protective pathways. Consequently, neurons exhibit reduced resistance to damage and toxicity, leading to accelerated apoptosis and neurodegeneration, thereby exacerbating HD progression.[34] DEFA5 plays a pivotal role in intestinal immune defense. By disrupting microbial cell membranes, DEFA5 directly inhibits the growth and spread of intestinal pathogens

https://doi.org/10.2147/IJGM.S511281

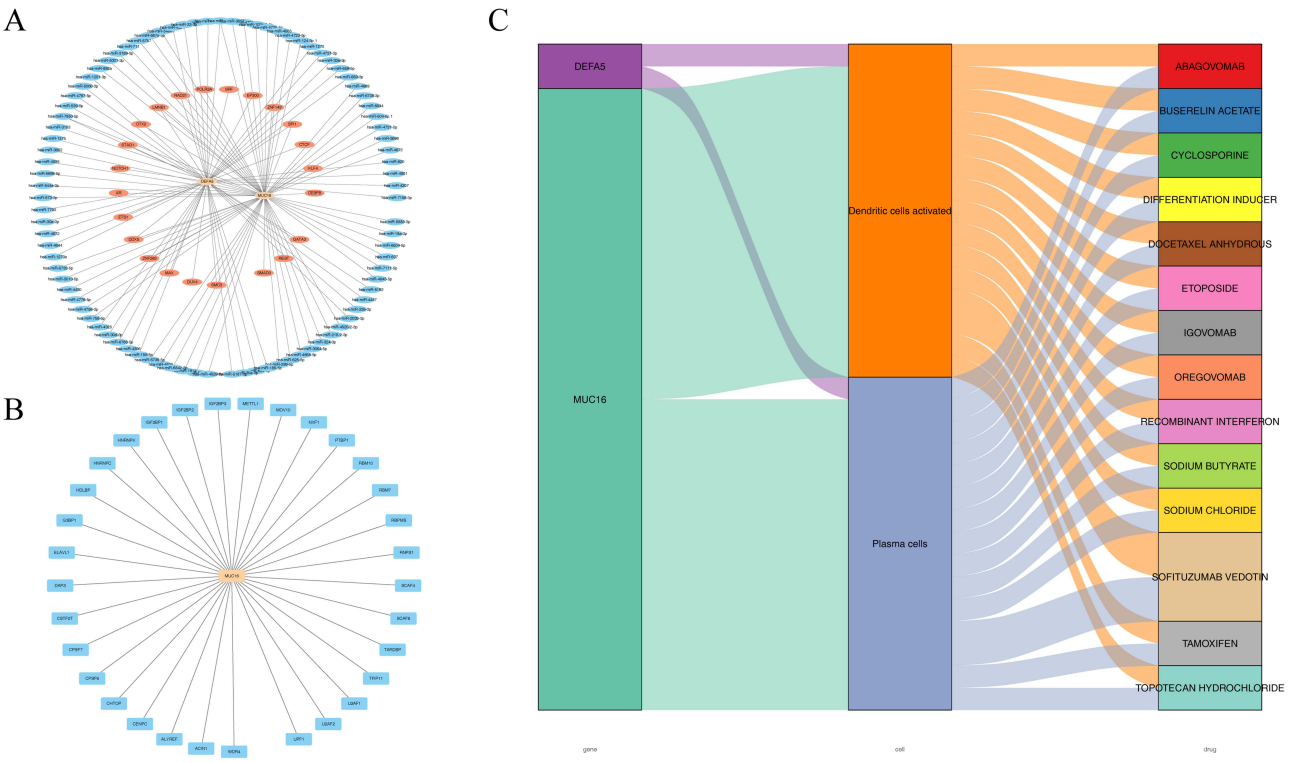

Figure 7 Construction of regulatory networks and drug prediction. (**A**) Key gene-miRNA-TF regulatory network diagram. In the network, Orange represents key genes, light orange represents transcription factors, and blue represents miRNAs. (**B**) Key gene-RBP interaction network diagram. In the network, orange represents key genes, and blue represents interacting RNA-binding proteins (RBPs). (**C**) Drug-key gene-immune cell network. The first column represents key genes, the second column represents differential immune cells, and the third column shows drugs predicted based on key genes.

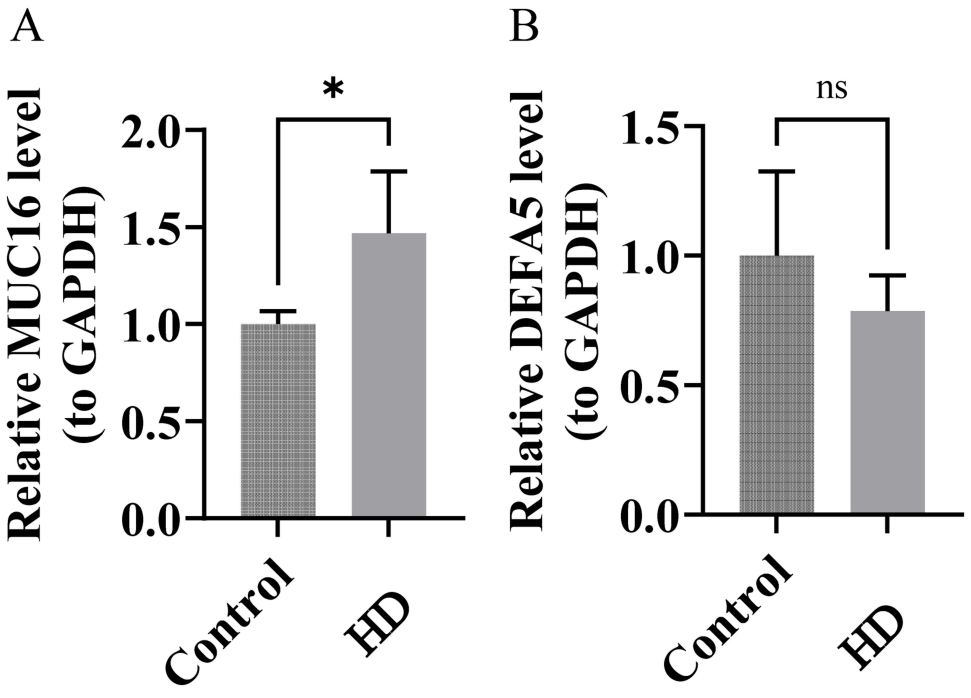

Figure 8 Expression of key genes. (**A**) Expression of the MUC16 gene in normal and disease groups. (**B**) Expression of the DEFA5 gene in normal and disease groups. An asterisk (*) was used to indicate that $P < 0.05$.

while maintaining the balance of the intestinal flora. Additionally, DEFA5 can regulate the functions of various immune cells. For example, it is capable of chemotaxing immune cells such as neutrophils, monocytes, and T lymphocytes to the site of inflammation, enhancing the body's immune defense response.[35] Beyond its role in immune barrier protection, DEFA5 is closely linked to the inflammatory response in the intestine. In inflammatory bowel diseases (IBD) such as Crohn's disease and ulcerative colitis, DEFA5 expression levels are often significantly altered, potentially affecting the integrity of the intestinal epithelial barrier and the severity of inflammation.[36] When HD-associated gene mutations alter the intestinal microenvironment, the secretion level of DEFA5 by Paneth cells may be dysregulated.[37] Abnormal DEFA5 levels could impair the maintenance of intestinal barrier function, allowing pathogens and harmful substances from the gut to enter systemic circulation more easily, thereby triggering systemic inflammation.[38] This inflammatory response may further propagate to the central nervous system (CNS) via circulation, exacerbating neuroinflammation and accelerating HD progression.[39] For instance, studies in HD animal models have demonstrated a strong correlation between gut inflammation and brain neuroinflammation, with DEFA5 dysregulation potentially serving as a critical link between the two.[40] In colorectal cancer research, abnormal DEFA5 expression has been associated with intestinal tumorigenesis and development. Changes in DEFA5 expression are thought to influence the proliferation, apoptosis, and carcinogenesis of intestinal epithelial cells by modulating the intestinal microenvironment and inflammatory responses. Downregulation of DEFA5 expression may weaken the intestine's resistance to pathogens, leading to a chronic inflammatory state and an increased risk of bowel cancer. In certain cases, overexpression of DEFA5 may also promote tumor development. Consequently, DEFA5 is regarded as a key molecular marker and potential therapeutic target in the study of intestinal diseases, particularly enteritis and colorectal cancer.[41] Notably, DEFA5 has been found to be expressed in the colonic mucosal crypts of patients with Crohn's colitis, and it has been suggested that it could serve as a biomarker for diagnosing colonic Crohn's colitis, with a positive predictive value as high as 96%.[42] *DEFA5* has also been identified as a risk factor for colorectal cancer in men following ulcerative colitis.[43] Additionally, differential DNA methylation of *DEFA5* may influence gene expression, contributing to the increased risk of necrotizing enterocolitis in preterm infants.[44] These findings suggest a strong association between *DEFA5* and inflammatory processes. Metabolic disorders, which can impact various diseases, also play a significant role in the pathogenesis of HD. These disorders may influence HD development and progression by affecting cell function, energy metabolism, and inflammatory responses.[45] Research has shown that DEFA5 can improve metabolic disorders and restore metabolic balance, potentially offering a protective role against HD35. In our study, *DEFA5* was found to predict the occurrence of HD. Furthermore, DEFA5 expression is significantly downregulated in gastric cancer, where it is the most downregulated gene in invasive gastric cancer. Overexpression of DEFA5 has been shown to reduce cell proliferation and tumor growth both in vitro and in vivo, suggesting its potential as a tumor suppressor in gastric cancer.[35,46] While DEFA5 may act as a risk factor in certain diseases, it could also have a therapeutic effect, and its role in HD requires further investigation.

MUC16, also known as CA125, is an immunosuppressive factor and a large transmembrane mucin produced by epithelial cells. It is abnormally elevated in various tumors.[47] Inflammation is closely linked to HD, and hemorrhoids are commonly observed in patients with cirrhosis. Studies have indicated that MUC16 serves as both a mediator and a marker of the inflammatory response,[48,49] playing a critical role in cirrhosis and its complications. Activated portal vein fibroblasts regulate cirrhosis via MUC16, and portal hypertension caused by MUC16 can obstruct venous return in the anorectal region. This leads to blood stasis, increased vascular pressure, and ultimately the formation of hemorrhoids.[50–52] This mechanism highlights MUC16's significant involvement in the development of hemorrhoids associated with cirrhosis. The cytoplasmic tail of MUC16 interacts with ERM family proteins (ezrin/radixin/moesin), thereby modulating cytoskeletal dynamics.[53] Notably, MUC16 suppresses natural killer (NK) cell responses, enabling cancer cells to evade immune attack.[54] In Huntington's disease (HD), aberrant immune activation is a hallmark feature.[55] MUC16 may disrupt immune surveillance and clearance of damaged neurons, perpetuating and amplifying neuroinflammatory responses that exacerbate HD progression.[56] Within the nervous system, MUC16 could impair neuron-neuron or neuron-glia interactions, inducing pathological glial migration and excessive neuronal ensheathment, which accelerates neurodegeneration.[57] Moreover, MUC16's immunomodulatory properties—mediated by its heavily glycosylated extracellular domain—allow it to bind diverse immune molecules.[57] Dysregulated MUC16 interferes with macrophage polarization and T-cell activation, fostering a pro-inflammatory milieu.[58] Additionally, aberrant MUC16 compromises

microenvironmental homeostasis, potentiating cell death and vascular integrity loss, which may aggravate hemorrhoidal pathogenesis.[59] In our study, *MUC16* was identified as a key gene for diagnosing HD. However, further clinical trials are required to validate its diagnostic utility.

This study developed a nomogram incorporating two key genes, achieving an AUC of 0.88. DCA revealed that the nomogram provided greater net benefit than individual key genes, demonstrating its robust predictive power and accuracy for HD. With an AUC surpassing 0.8, the nomogram consistently outperformed individual genes in DCA, indicating its strong predictive potential for HD incidence. This represents a novel finding, as few related studies exist. Our research addresses this gap and offers a valuable decision-support tool for HD in clinical practice.

The peroxisome pathway, essential in cellular metabolism, has been linked to enteritis and possibly hemorrhoids, suggesting that disturbances in this pathway may contribute to enteritis development, which in turn impacts overall health.[60,61] Research on the starch and sucrose metabolic pathway indicates that sugar metabolism influences diabetes progression and elevates the risk of diseases like HD, implying that disruptions in this pathway may indirectly contribute to other conditions by triggering diabetes.[62] Although the progression of juvenile diabetes is not fully elucidated, it is hypothesized to be closely associated with diabetes pathogenesis and potentially linked to other diseases.[63] The cytokine-cytokine receptor interaction pathway plays a key role in the inflammatory response, influencing HD by regulating inflammation and impacting disease progression.[64,65] These findings provide compelling evidence for the involvement of these pathways in disease development, offering valuable insights and guiding future research directions. Based on pathway analysis and supporting literature, it can be inferred that MUC16 and DEFA5 may modulate inflammatory responses, glucose metabolism, energy metabolism, and other pathways, potentially influencing HD. These genes may play pivotal roles in regulating these pathways, thereby affecting HD through the modulation of inflammation, energy metabolism, and related processes. However, this remains a hypothesis derived from GSEA enrichment results and literature analysis, and the precise relationship and mechanisms warrant further experimental validation. In conclusion, this paper outlines a potential mechanism for MUC16 and DEFA5 in HD, offering valuable insights and directions for future research.

Accumulating evidence underscores the immunomodulatory roles of MUC16 and DEFA5 across pathologies. In ovarian cancer, MUC16 inhibits the cytolytic activity of natural killer (NK) cells by impeding the formation of NK cell-tumor cell conjugates, thereby facilitating immune evasion.[57] By analogy, in Huntington's disease (HD), MUC16 may similarly dysregulate immune cell secretion of pro-inflammatory cytokines (eg, IL-1β, TNF-α), highlighting its broader immunoregulatory potential.[66] While studies on DEFA5 in HD remain limited, emerging data suggest it may modulate central nervous system (CNS) immune cells, influencing the release of IL-1β and TNF-α.[67] Parallel findings in colorectal cancer reveal that microbiota-derived metabolites can shape disease progression by altering immune cell function,[68,69] offering a conceptual framework for investigating DEFA5's role in HD via analogous immunometabolic mechanisms. Analysis revealed that activated dendritic cells exhibited low infiltration in HD, while plasma cells showed high infiltration. Notably, plasma cells displayed a strong positive correlation with DEFA5 (cor = 0.5321). The reduced function of activated dendritic cells may result in insufficient or dysregulated cytokine secretion, either pro-inflammatory or anti-inflammatory, potentially contributing to localized inflammation in hemorrhoids.[70] The high infiltration of plasma cells in HD suggests persistent inflammation,[71] indicating that both activated dendritic cells and plasma cells may play significant roles in exacerbating local inflammatory responses and HD progression. The NF-κB pathway serves as a central signaling axis in immune and inflammatory responses.[72] Accumulating evidence indicates that members of the defensin family, including DEFA5, can interact with the NF-κB pathway.[73] For instance, in certain inflammatory models, bacterial defensins activate the NF-κB pathway, upregulating the expression of pro-inflammatory cytokines. Specifically, DEFA5 may influence plasma cells through a similar mechanism.[74] Studies have demonstrated that NF-κB activation under inflammatory stimuli promotes B-cell differentiation into plasma cells and enhances antibody secretion,[75] providing indirect evidence for DEFA5's role in modulating plasma cells via NF-κB. Moreover, DEFA5 may function as an endogenous ligand, binding to Toll-like receptors (TLRs) on immune cells and initiating TLR-mediated signaling.[76] This pathway's activation could critically regulate plasma cell differentiation,[77] suggesting a potential mechanistic link between DEFA5 and humoral immune responses.

However, this study has several limitations. First, only a few key modules and associated genes were considered, potentially overlooking other relevant HD-associated genes. Second, the dataset utilized included samples from individuals treated with biological agents, and the impact of these treatments on gene expression remains unclear. The impact of reagent impurities, batch differences, and other factors on the results should be considered. In future experimental designs, multiple parallel samples should be set up, using reagents from the same batch, ensuring thorough mixing before each experiment, and including positive and negative controls to reduce reagent interference with the experimental results. Additionally, the exact mechanisms by which central genes, Incrnas, and miRNAs influence HD were not explored.

This research identified two key genes, *MUC16* and *DEFA5*, associated with HD and MAM, and developed a nomogram with strong predictive capabilities. These findings provide new targets for exploring the pathogenesis and treatment of HD. However, the clinical applicability and effectiveness of these key genes require further validation and investigation.

Abbreviations

HD, Hemorrhoidal Disease; MAM, Mitochondria-Associated Membranes; DEFA5, Defensin Alpha 5; MAM-RGs, MAM-related genes; GEO, Gene Expression Omnibus; ssGSEA, Single-sample Gene Set Enrichment Analysis; LASSO, Least Absolute Shrinkage and Selection Operator; PPI, Protein-Protein Interaction; RT-qPCR, Reverse transcription-quantitative PCR; DEGs, Differentially expressed genes; ER, Endoplasmic reticulum; FC, Fold change; GO, Gene Ontology; KEGG, Kyoto Encyclopedia of Genes and Genomes; STRING, Search Tool for the Retrieval of Interacting Genes website; LASSO, Least Absolute Shrinkage and Selection Operator; BP, Biological process; CC, Cellular component; MF, Molecular function; DEFA5, Defensin Alpha 5; MUC16, Mucin 16; IBD, Inflammatory Bowel Disease.

Data Sharing Statement

The datasets analyzed in this study are available in the Gene Expression Omnibus (GEO) database (https://www.ncbi.nlm.nih.gov/geo/).

Ethics Approval Statement

We certify that the research study titled "Identification and validation of key genes involved in the coupling of mitochondria-associated endoplasmic reticulum membrane in hemorrhoidal disease" has been approved by the Ethics Committee of Jiangxi Provincial People's Hospital. The approval number and date of approval are as follows: 2024(77), November 1st, 2024. The study of clinical samples was in compliance with the Declaration of Helsinki.

Patient Consent Statement

Participants in this study were provided with a clear and understandable explanation of the research objectives, procedures, potential risks, and benefits. They were informed that their participation is voluntary and that they have the right to withdraw from the study at any time. Participants were given the opportunity to ask questions and provided written informed consent prior to their involvement in the study.

Author Contributions

Lihua Mao took part in drafting, Zhiying Rao revising or critically reviewing the article, Yanru Wang gave final approval of the version to be published; Jun Yang and Junmei He have agreed on the journal to which the article has been submitted; Zhi Zheng and Lanyu Chen agree to be accountable for all aspects of the work. All authors made a significant contribution to the work reported, whether that is in the conception, study design, execution, acquisition of data, analysis and interpretation, or in all these areas; took part in drafting, revising or critically reviewing the article; gave final approval of the version to be published; have agreed on the journal to which the article has been submitted; and agree to be accountable for all aspects of the work.

Funding

This study was supported by the Jiangxi Provincial Administration of Traditional Chinese Medicine Fund Project (grant no. 2024B0143, 2022B392).

Disclosure

The authors report no conflicts of interest in this work.

References

1. Riss S, Weiser FA, Schwameis K, et al. The prevalence of hemorrhoids in adults. *Int J Colorectal Dis*. 2012;27(2):215–220. doi:10.1007/s00384-011-1316-3
2. Gallo G, Martellucci J, Sturiale A, et al. Consensus statement of the Italian society of colorectal surgery (SICCR): management and treatment of hemorrhoidal disease. *Tech Coloproctol*. 2020;24(2):145–164. doi:10.1007/s10151-020-02149-1
3. Lohsiriwat V, Sheikh P, Bandolon R, et al. Recurrence rates and pharmacological treatment for hemorrhoidal disease: a systematic review. *Adv Ther*. 2023;40(1):117–132. doi:10.1007/s12325-022-02351-7
4. Wu EB, Sung FC, Lin CL, Wu KL, Chen KB. Colorectal cancer risk in patients with hemorrhoids: a 10-year population-based retrospective cohort study. *Int J Environ Res Public Health*. 2021;18(16):8655. doi:10.3390/ijerph18168655
5. Hsu SP, Chen HH, Wang TY, et al. Association of hemorrhoids with Hashimoto's thyroiditis and associated comorbidities: a nationwide population-based cohort study. *Front Endocrinol*. 2020;11:577767. doi:10.3389/fendo.2020.577767
6. Dekker L, Han-Geurts IJM, Rorvik HD, van Dieren S, Bemelman WA. Rubber band ligation versus haemorrhoidectomy for the treatment of grade II-III haemorrhoids: a systematic review and meta-analysis of randomised controlled trials. *Tech Coloproctol*. 2021;25(6):663–674. doi:10.1007/s10151-021-02430-x
7. Mao H, Chen W, Chen L, Li L. Potential role of mitochondria-associated endoplasmic reticulum membrane proteins in diseases. *Biochem Pharmacol*. 2022;199:115011. doi:10.1016/j.bcp.2022.115011
8. Wang WX, Prajapati P, Nelson PT, Springer JE. The mitochondria-associated ER membranes are novel subcellular locations enriched for inflammatory-responsive MicroRNAs. *Mol Neurobiol*. 2020;57(7):2996–3013. doi:10.1007/s12035-020-01937-y
9. Stacchiotti A. Exploring cellular stress response and chaperones. *Cells*. 2019;8(5):408. doi:10.3390/cells8050408
10. Ding Y, Liu N, Zhang D, et al. Mitochondria-associated endoplasmic reticulum membranes as a therapeutic target for cardiovascular diseases. *Front Pharmacol*. 2024;15:1398381. doi:10.3389/fphar.2024.1398381
11. Theurey P, Rieusset J. Mitochondria-associated membranes response to nutrient availability and role in metabolic diseases. *Trends Endocrinol Metab*. 2017;28(1):32–45. doi:10.1016/j.tem.2016.09.002
12. Nandi A, Nigar T, Das A, Dey YN. Network pharmacology analysis of Plumbago zeylanica to identify the therapeutic targets and molecular mechanisms involved in ameliorating hemorrhoids. *J Biomol Struct Dyn*. 2023;1–15. doi:10.1080/07391102.2023.2280681
13. Chen Y, Xia S, Zhang L, et al. Mitochondria-associated endoplasmic reticulum membrane (MAM) is a promising signature to predict prognosis and therapies for hepatocellular carcinoma (HCC). *J Clin Med*. 2023;12(5):1830. doi:10.3390/jcm12051830
14. Love MI, Huber W, Anders S. Moderated estimation of fold change and dispersion for RNA-seq data with DESeq2. *Genome Biol*. 2014;15(12):550. doi:10.1186/s13059-014-0550-8
15. Wang J, Wu N, Feng X, et al. PROS1 shapes the immune-suppressive tumor microenvironment and predicts poor prognosis in glioma. *Front Immunol*. 2022;13:1052692. doi:10.3389/fimmu.2022.1052692
16. Zhao P, Zhen H, Zhao H, Huang Y, Cao B. Identification of hub genes and potential molecular mechanisms related to radiotherapy sensitivity in rectal cancer based on multiple datasets. *J Transl Med*. 2023;21(1):176. doi:10.1186/s12967-023-04029-2
17. Chen H, Boutros PC. VennDiagram: a package for the generation of highly-customizable Venn and Euler diagrams in R. *BMC Bioinf*. 2011;12:35. doi:10.1186/1471-2105-12-35
18. Wu T, Hu E, Xu S, et al. clusterProfiler 4.0: a universal enrichment tool for interpreting omics data. *Innovation*. 2021;2(3):100141. doi:10.1016/j.xinn.2021.100141
19. Shannon P, Markiel A, Ozier O, et al. Cytoscape: a software environment for integrated models of biomolecular interaction networks. *Genome Res*. 2003;13(11):2498–2504. doi:10.1101/gr.1239303
20. Friedman J, Hastie T, Tibshirani R. Regularization paths for generalized linear models via coordinate descent. *J Stat Softw*. 2010;33(1):1–22.
21. Robin X, Turck N, Hainard A, et al. pROC: an open-source package for R and S+ to analyze and compare ROC curves. *BMC Bioinf*. 2011;12:77. doi:10.1186/1471-2105-12-77
22. Wang L, Shen J, Wang Y, Bi J. Identification of fatty acid metabolism-based molecular subtypes and prognostic signature to predict immune landscape and guide clinical drug treatment in renal clear cell carcinoma. *Int Immunopharmacol*. 2023;116:109735. doi:10.1016/j.intimp.2023.109735
23. Liu TT, Li R, Huo C, et al. Identification of CDK2-related immune forecast model and ceRNA in lung adenocarcinoma, a pan-cancer analysis. *Front Cell Dev Biol*. 2021;9:682002. doi:10.3389/fcell.2021.682002
24. Sun T, Cao Y, Huang T, Sang Y, Dai Y, Tao Z. Comprehensive analysis of fifteen hub genes to identify a promising diagnostic model, regulated networks, and immune cell infiltration in acute kidney injury. *J Clin Lab Anal*. 2022;36(11):e24709. doi:10.1002/jcla.24709
25. Chen B, Khodadoust MS, Liu CL, Newman AM, Alizadeh AA. Profiling tumor infiltrating immune cells with CIBERSORT. *Methods Mol Biol*. 2018;1711:243–259. doi:10.1007/978-1-4939-7493-1_12
26. Tolomeo K; Joint Commission on Hospital A. More on managing hazardous materials and waste. A further examination into EC.02.02.01. *Jt Comm Perspect*. 2016;36(1):13–14.
27. Mangiola S, Doyle MA, Papenfuss AT. Interfacing Seurat with the R tidy universe. *Bioinformatics*. 2021;37(22):4100–4107. doi:10.1093/bioinformatics/btab404

28. He Q, Yang J, Pan Z, et al. Biochanin A protects against iron overload associated knee osteoarthritis via regulating iron levels and NRF2/System xc-/GPX4 axis. *Biomed Pharmacother*. 2023;157:113915. doi:10.1016/j.biopha.2022.113915
29. Cheng F, Luk AO, Tam CHT, et al. Shortened relative leukocyte telomere length is associated with prevalent and incident cardiovascular complications in type 2 diabetes: analysis from the Hong Kong diabetes register. *Diabetes Care*. 2020;43(9):2257–2265. doi:10.2337/dc20-0028
30. Soares TR, Reis SD, Pinho BR, Duchen MR, Oliveira JMA. Targeting the proteostasis network in Huntington's disease. *Ageing Res Rev*. 2019;49:92–103. doi:10.1016/j.arr.2018.11.006
31. Bayram-Weston Z, Jones L, Dunnett SB, Brooks SP. Comparison of mHTT antibodies in Huntington's disease mouse models reveal specific binding profiles and steady-state Ubiquitin levels with disease development. *PLoS One*. 2016;11(5):e0155834. doi:10.1371/journal.pone.0155834
32. Cavanaugh JE. Role of extracellular signal regulated kinase 5 in neuronal survival. *Eur J Biochem*. 2004;271(11):2056–2059. doi:10.1111/j.1432-1033.2004.04131.x
33. Asl ER, Amini M, Najafi S, et al. Interplay between MAPK/ERK signaling pathway and MicroRNAs: a crucial mechanism regulating cancer cell metabolism and tumor progression. *Life Sci*. 2021;278:119499. doi:10.1016/j.lfs.2021.119499
34. Ziv NE, Ciechanover A. A possible non-proteolytic role of ubiquitin conjugation in alleviating the pathology of Huntingtin's aggregation. *Cell Death Differ*. 2021;28(2):814–817. doi:10.1038/s41418-020-00617-7
35. Wu Z, Ding Z, Cheng B, Cui Z. The inhibitory effect of human DEFA5 in growth of gastric cancer by targeting BMI1. *Cancer Sci*. 2021;112(3):1075–1083. doi:10.1111/cas.14827
36. Hu X, Deng J, Yu T, et al. ATF4 deficiency promotes intestinal inflammation in mice by reducing uptake of glutamine and expression of antimicrobial peptides. *Gastroenterology*. 2019;156(4):1098–1111. doi:10.1053/j.gastro.2018.11.033
37. Ouellette AJ. Paneth cell α-defensins in enteric innate immunity. *Cell Mol Life Sci*. 2011;68(13):2215–2229. doi:10.1007/s00018-011-0714-6
38. Acioglu C, Elkabes S. Innate immune sensors and regulators at the blood brain barrier: focus on toll-like receptors and inflammasomes as mediators of neuro-immune crosstalk and inflammation. *J Neuroinflammation*. 2025;22(1):39. doi:10.1186/s12974-025-03360-3
39. Jensen SB, Sheikh MA, Akkouh IA, et al. Elevated systemic levels of markers reflecting intestinal barrier dysfunction and inflammasome activation are correlated in severe mental illness. *Schizophr Bull*. 2023;49(3):635–645. doi:10.1093/schbul/sbac191
40. Liu X, Liu Y, Liu J, et al. Correlation between the gut microbiome and neurodegenerative diseases: a review of metagenomics evidence. *Neural Regen Res*. 2024;19(4):833–845. doi:10.4103/1673-5374.382223
41. Qiao Q, Bai R, Song W, et al. Human alpha-defensin 5 suppressed colon cancer growth by targeting PI3K pathway. *Exp Cell Res*. 2021;407(2):112809. doi:10.1016/j.yexcr.2021.112809
42. Rana T, Korolkova OY, Rachakonda G, et al. Linking bacterial enterotoxins and alpha defensin 5 expansion in the Crohn's colitis: a new insight into the etiopathogenetic and differentiation triggers driving colonic inflammatory bowel disease. *PLoS One*. 2021;16(3):e0246393. doi:10.1371/journal.pone.0246393
43. Taman H, Fenton CG, Hensel IV, Anderssen E, Florholmen J, Paulssen RH. Transcriptomic landscape of treatment-naive ulcerative colitis. *J Crohn's Colitis*. 2018;12(3):327–336. doi:10.1093/ecco-jcc/jjx139
44. Klerk DH, Plosch T, Verkaik-Schakel RN, Hulscher JBF, Kooi EMW, Bos AF. DNA methylation of TLR4, VEGFA, and DEFA5 is associated with necrotizing enterocolitis in preterm infants. *Front Pediatr*. 2021;9:630817. doi:10.3389/fped.2021.630817
45. Chiang CP, Jao SW, Lee SP, et al. Expression pattern, ethanol-metabolizing activities, and cellular localization of alcohol and aldehyde dehydrogenases in human large bowel: association of the functional polymorphisms of ADH and ALDH genes with hemorrhoids and colorectal cancer. *Alcohol*. 2012;46(1):37–49. doi:10.1016/j.alcohol.2011.08.004
46. Nagao S, Takahashi Y, Denda T, et al. Reduced DEFA5 expression and STAT3 activation underlie the submucosal invasion of early gastric cancers. *Digestion*. 2023;104(6):480–493. doi:10.1159/000531790
47. Song Y, Yuan M, Wang G. Update value and clinical application of MUC16 (cancer antigen 125). *Expert Opin Ther Targets*. 2023;27(8):745–756. doi:10.1080/14728222.2023.2248376
48. Katoh M. Multi-layered prevention and treatment of chronic inflammation, organ fibrosis and cancer associated with canonical WNT/beta-catenin signaling activation (Review). *Int J Mol Med*. 2018;42(2):713–725. doi:10.3892/ijmm.2018.3689
49. Nunez J, de la Espriella R, Minana G, et al. Antigen carbohydrate 125 as a biomarker in heart failure: a narrative review. *Eur J Heart Fail*. 2021;23(9):1445–1457. doi:10.1002/ejhf.2295
50. Koyama Y, Wang P, Liang S, et al. Mesothelin/mucin 16 signaling in activated portal fibroblasts regulates cholestatic liver fibrosis. *J Clin Invest*. 2017;127(4):1254–1270. doi:10.1172/JCI88845
51. Gines P, Krag A, Abraldes JG, Sola E, Fabrellas N, Kamath PS. Liver cirrhosis. *Lancet*. 2021;398(10308):1359–1376. doi:10.1016/S0140-6736(21)01374-X
52. Galati G, De Vincentis A, Ripetti V, et al. Haemorrhoidal disease in severe portal hypertension: a combined approach with transjugular intrahepatic portosystemic shunt (TIPS) and transanal haemorrhoidal dearterialization (THD). *Arch Med Sci*. 2014;10(1):195–196. doi:10.5114/aoms.2014.40746
53. Zhang XY, Hong LL, Ling ZQ. MUC16: clinical targets with great potential. *Clin Exp Med*. 2024;24(1):101. doi:10.1007/s10238-024-01365-5
54. Belisle JA, Horibata S, Jennifer GAA, et al. Identification of Siglec-9 as the receptor for MUC16 on human NK cells, B cells, and monocytes. *Mol Cancer*. 2010;9(1):118. doi:10.1186/1476-4598-9-118
55. Li X, Tong H, Xu S, et al. Neuroinflammatory proteins in Huntington's disease: insights into mechanisms, diagnosis, and therapeutic implications. *Int J Mol Sci*. 2024;25(21):11787. doi:10.3390/ijms252111787
56. Zhang L, Han X, Shi Y. Association of MUC16 mutation with response to immune checkpoint inhibitors in solid tumors. *JAMA Network Open*. 2020;3(8):e2013201. doi:10.1001/jamanetworkopen.2020.13201
57. Gubbels JA, Felder M, Horibata S, et al. MUC16 provides immune protection by inhibiting synapse formation between NK and ovarian tumor cells. *Mol Cancer*. 2010;9:11. doi:10.1186/1476-4598-9-11
58. Rodríguez JP, Casas J, Balboa MA, Balsinde J. Bioactive lipid signaling and lipidomics in macrophage polarization: impact on inflammation and immune regulation. *Front Immunol*. 2025;16:1550500. doi:10.3389/fimmu.2025.1550500
59. Hu J, Sun J. MUC16 mutations improve patients' prognosis by enhancing the infiltration and antitumor immunity of cytotoxic T lymphocytes in the endometrial cancer microenvironment. *Oncoimmunology*. 2018;7(10):e1487914. doi:10.1080/2162402x.2018.1487914

60. O'Morain C, Smethurst P, Levi AJ, Peters TJ. Organelle pathology in ulcerative and Crohn's colitis with special reference to the lysosomal alterations. *Gut*. 1984;25(5):455–459. doi:10.1136/gut.25.5.455
61. Venkataraman B, Ojha S, Belur PD, et al. Phytochemical drug candidates for the modulation of peroxisome proliferator-activated receptor gamma in inflammatory bowel diseases. *Phytother Res*. 2020;34(7):1530–1549. doi:10.1002/ptr.6625
62. Poznyak A, Grechko AV, Poggio P, Myasoedova VA, Alfieri V, Orekhov AN. The diabetes mellitus-atherosclerosis connection: the role of lipid and glucose metabolism and chronic inflammation. *Int J Mol Sci*. 2020;21(5):1835. doi:10.3390/ijms21051835
63. Zheng Y, Zhang G, Chen Z, Zeng Q. Relationship between type 2 diabetes and inflammation diseases: cohort study in Chinese adults. *Iran J Public Health*. 2015;44(8):1045–1052.
64. Dong Q, Han Z, Tian L. Identification of serum exosome-derived circRNA-miRNA-TF-mRNA regulatory network in postmenopausal osteoporosis using bioinformatics analysis and validation in peripheral blood-derived mononuclear cells. *Front Endocrinol*. 2022;13:899503. doi:10.3389/fendo.2022.899503
65. Wu S, Yang S, Li R, et al. HSV-1 infection-induced herpetic neuralgia involves a CCL5/CCR5-mediated inflammation mechanism. *J Med Virol*. 2023;95(4):e28718. doi:10.1002/jmv.28718
66. Felder M, Kapur A, Rakhmilevich AL, et al. MUC16 suppresses human and murine innate immune responses. *Gynecol Oncol*. 2019;152(3):618–628. doi:10.1016/j.ygyno.2018.12.023
67. Watashi K, Liang G, Iwamoto M, et al. Interleukin-1 and tumor necrosis factor-α trigger restriction of hepatitis B virus infection via a cytidine deaminase activation-induced cytidine deaminase (AID). *J Biol Chem*. 2013;288(44):31715–31727. doi:10.1074/jbc.M113.501122
68. Alharbi KS, Alenezi SK, Alsahli T, et al. Effect of sakuranetin against cyclophosphamide-induced immunodeficiency mice: role of IFN-γ/TNF-α/IgG/IgM/interleukins. *Naunyn Schmiedebergs Arch Pharmacol*. 2025:1–2. doi:10.1007/s00210-025-03988-1
69. O'Carroll SJ, Kho DT, Wiltshire R, et al. Pro-inflammatory TNFα and IL-1β differentially regulate the inflammatory phenotype of brain microvascular endothelial cells. *J Neuroinflammation*. 2015;12:131. doi:10.1186/s12974-015-0346-0
70. Ikeda Y, Akbar SM, Matsui H, Murakami H, Onji M. Depletion and decreased function of antigen-presenting dendritic cells caused by lymphocytapheresis in ulcerative colitis. *Dis Colon Rectum*. 2003;46(4):521–528. doi:10.1007/s10350-004-6593-2
71. Sapp M, Perez-Ordonez B, Brenneman F, Imrie K, Morava-Protzner I, Lim MS. EBV-associated perianal Hodgkin's disease in an HIV-positive individual. *Am J Hematol*. 2001;66(1):42–45. doi:10.1002/1096-8652(200101)66:1<42::AID-AJH1006>3.0.CO;2-V
72. Huang C, Sun Y, Qiu X, et al. The intracellular interaction of porcine β-Defensin 2 with VASH1 alleviates inflammation via Akt signaling pathway. *J Immunol*. 2022;208(12):2795–2805. doi:10.4049/jimmunol.2100810
73. Kanoh H, Iwashita S, Kuraishi T, et al. cGMP signaling pathway that modulates NF-κB activation in innate immune responses. *iScience*. 2021;24(12):103473. doi:10.1016/j.isci.2021.103473
74. Lawrence T. The nuclear factor NF-kappaB pathway in inflammation. *Cold Spring Harb Perspect Biol*. 2009;1(6):a001651. doi:10.1101/cshperspect.a001651
75. Sasaki Y, Iwai K. Roles of the NF-κB pathway in B-lymphocyte biology. *Curr Top Microbiol Immunol*. 2016;393:177–209. doi:10.1007/82_2015_479
76. Moynagh PN. TLR signalling and activation of IRFs: revisiting old friends from the NF-kappaB pathway. *Trends Immunol*. 2005;26(9):469–476. doi:10.1016/j.it.2005.06.009
77. Liu Z, Liu Y, Li T, et al. CMTM7 plays key roles in TLR-induced plasma cell differentiation and p38 activation in murine B-1 B cells. *Eur J Immunol*. 2020;50(6):809–821. doi:10.1002/eji.201948363